**Proceedings of the Estonian Academy of Sciences**
2026, **75**, 4, 346–352

https://doi.org/10.3176/proc.2026.4.08

www.eap.ee/proceedings
Estonian Academy Publishers

ELECTRIC MACHINE THERMAL MANAGEMENT, TOPOLOGY OPTIMIZATION

RESEARCH ARTICLE

Received 7 July 2026
Accepted 22 September 2026
Available online 2 November 2026

**Keywords:**
electric machine cooling, topology optimization, additive manufacturing, cooling channels, reduced-order modeling

**Corresponding author:**
Yang Zhang
yang.zhang@taltech.ee

**Citation:**
Zhang, Y., Sarap, M., Vaimann, T. and Kallaste, A. 2026. Additive manufacturing-aware topology optimization of cooling channels using a reduced-order cold plate model for electric machine water jackets. *Proceedings of the Estonian Academy of Sciences*, **75**(4), 346–352. https://doi.org/10.3176/proc.2026.4.08

© 2026 Authors. This is an open access article distributed under the terms and conditions of the Creative Commons Attribution (CC BY) license (http://creativecommons.org/licenses/by/4.0).

# Additive manufacturing-aware topology optimization of cooling channels using a reduced-order cold plate model for electric machine water jackets

Yang Zhang, Martin Sarap, Toomas Vaimann and Ants Kallaste

Department of Electrical Power Engineering and Mechatronics, Tallinn University of Technology, Ehitajate tee 5, 19086 Tallinn, Estonia

## ABSTRACT

Integrated liquid cooling jackets are widely used in the thermal management of high-power-density motors, but traditional designs rely on parametric channel layouts, failing to fully utilize the geometric degrees of freedom offered by additive manufacturing (AM). This paper proposes an AM-aware topology optimization framework based on a reduced-order cold plate model. A two-dimensional case study systematically investigates the effects of manufacturability-oriented regularization on channel topology and thermo-hydraulic performance. Results show that stronger regularization substantially reduces interface complexity and fluid area fraction, while generally increasing hydraulic resistance and degrading thermal performance. A sharp-interface reanalysis further demonstrates good agreement in the global thermal response, while revealing the sensitivity of the local peak temperature and hydraulic conductance to the density-based representation.

## 1. Introduction

The continuous increase in the power density of modern electric machines has intensified the demand for effective thermal management solutions. Excessive operating temperatures can accelerate insulation ageing, reduce efficiency, and limit achievable power density. Accordingly, liquid-cooled water jackets have become one of the most widely adopted cooling technologies in high-performance electric machines due to their high heat-removal capability and ease of integration into the machine housing [1,2].

Conventional water jacket designs generally implement a defined geometric layout (a helical, serpentine, or circumferential type of flow), and their design freedoms are limited by their traditional production lines. Therefore, geometric optimization for improved thermal performance has only limited prospects.

In recent years, advancements in additive manufacturing (AM) have dramatically expanded the field of manufacturable internal cooling structures. Complex flow paths, detailed channel networks, and highly integrated cooling features can now be built with a degree of geometric variation that is challenging or impossible through conventional manufacturing processes. This development has motivated growing interest in topology optimization (TO) as a design tool for next-generation thermal management systems.

TO has demonstrated considerable potential for generating high-performance cooling structures by automatically distributing fluid and solid regions according to a specified objective function [3]. However, unconstrained TO frequently produces highly complex geometries containing fine features, disconnected regions, and fragmented channel networks that are difficult to manufacture in practice. Consequently, the integration of manufacturability considerations into the TO process has become an important research challenge.

For electric machine cooling applications, this challenge is particularly relevant because the manufacturability of internal water jacket structures directly affects the feasibility of implementing topology-optimized designs. Nevertheless, direct TO of a complete three-dimensional water jacket remains computationally expensive and complicates the systematic investigation of manufacturing-related constraints.

To address this issue, this paper proposes an AM-aware TO framework based on a reduced-order cold plate abstraction of an electric machine water jacket. The framework combines density-based TO with manufacturability-oriented regularization techniques, including Helmholtz filtering, Heaviside projection, and perimeter regularization. A series of numerical case studies is conducted to investigate how these regularization mechanisms influence channel topology, thermal performance, hydraulic behavior, and geometric complexity. The objective is not to obtain a final industrial design but rather to establish a computationally efficient methodology for exploring the trade-off among thermal performance, hydraulic behavior, and manufacturability in topology-optimized cooling systems.

## 2. Methodology

Figure 1 provides an overview of the proposed AM-aware TO framework for cooling channel design.

First, the integrated water jacket is abstracted into a reduced-order liquid cooling plate model to improve computational efficiency. Second, a density-based TO method is applied to generate the cooling channel layout with the goal of minimizing the average temperature. Third, manufacturability constraints are progressively strengthened by controlling the minimum feature size and incorporating additional perimeter penalties. Finally, the resulting topology is evaluated to assess its structural feasibility and thermal performance.

### 2.1. Cold plate abstraction of a water jacket

To investigate the influence of AM-oriented regularization on cooling channel topology at reduced computational cost, the housing-integrated water jacket is represented by a two-dimensional cold plate model. The reduction is based on the incompressible Navier–Stokes and energy equations under the assumption that the dominant topology evolution and coolant redistribution occur in the in-plane directions, while the through-thickness velocity component and field variations are secondary during the conceptual design stage.

Considering the three-dimensional velocity field $u = (u, v, w)$, the reduced-order formulation assumes $w \approx 0$ and $\partial(\cdot)/\partial z \approx 0$. Under these assumptions, the three-dimensional continuity equation reduces to

$$\frac{\partial u}{\partial x} + \frac{\partial v}{\partial y} = 0, \tag{1}$$

while the in-plane momentum and energy equations retain the coupled effects of pressure-driven flow, viscous transport, Brinkman penalization, heat conduction, and convective heat transfer. The prescribed out-of-plane thickness $L$ is retained when evaluating integral quantities such as the volumetric flow rate.

The representative jacket thickness is 10 mm, whereas the in-plane dimensions of the reduced design domain are 120 mm × 50 mm. The resulting domain, shown in Fig. 2, contains fixed inlet and outlet regions of 10 mm × 5 mm, while the central region forms the TO domain in which the fluid and solid distributions are allowed to evolve.

The present reduction is intended as a topology development model rather than a complete representation of a practical three-dimensional motor water jacket. Through-thickness velocity and temperature gradients, three-dimensional manifold effects, secondary flows, and local housing features are therefore not explicitly resolved. Accordingly, the model is primarily used to compare relative topology and performance trends under identical thermal and hydraulic conditions rather than to provide direct quantitative predictions for a specific production water jacket.

### 2.2. Governing equations and boundary conditions

Following the reduced-order assumptions introduced in Section 2.1, the fluid domain is modeled using the two-dimensional incompressible laminar Navier–Stokes equations with Brinkman penalization. To suppress flow within solid regions, a Brinkman penalization term is introduced into the momentum equations. The governing equations are expressed as

$$\nabla \cdot u = 0, \tag{2}$$

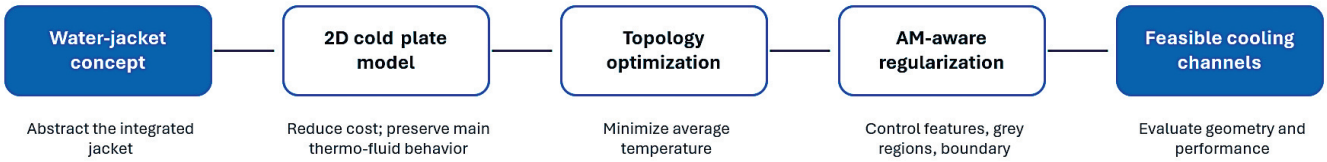



**Fig.1.** Overview of the proposed AM-aware TO framework for cooling channel design using a cold plate abstraction.

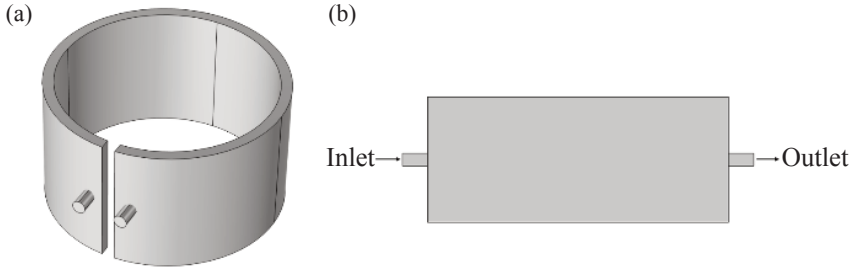



**Fig. 2.** Conceptual illustration of the water jacket cooling structure and its reduced-order abstraction: (a) housing-integrated water jacket, (b) corresponding liquid cold plate model with defined inlet and outlet boundaries.

$$\rho_f(u \cdot \nabla)\mathrm{u} = -\nabla p + \mu_f \nabla^2 u - \alpha(\rho)u, \tag{3}$$

where $u$ represents the velocity, $p$ represents the pressure, $\rho_f$ represents the fluid density, $\mu_f$ represents the dynamic viscosity, and $\alpha$ ($\rho$) is the Brinkman penalization coefficient. Here, transfer is governed by coupled convection and conduction:

$$\rho C_p(u \cdot \nabla T) = \nabla \cdot (k\nabla T) + Q, \tag{4}$$

where $T$ represents the temperature, $k$ represents the thermal conductivity, $C_p$ represents the specific heat capacity, and $Q$ is the volumetric heat source.

The thermo-fluid model employs water as the coolant and steel as the solid material. The corresponding material properties and the Brinkman penalization coefficient are summarized in Table 1.

A pressure difference drives the flow through the domain. The inlet pressure is prescribed as 2 Pa, while the outlet pressure is fixed at 0 Pa, resulting in the same pressure difference for all optimization cases. This relatively low pressure difference is intentionally used as a reduced-order benchmark condition to maintain a stable laminar flow regime and to enable consistent comparison of topology-dependent hydraulic behavior under identical driving conditions. It is not intended to represent the full pressure drop of a practical motor cooling circuit.

The coolant enters the domain at 293.15 K. All external boundaries are assumed adiabatic, and heat exchange with the surrounding air is neglected. A total heat rate of 50 W is applied uniformly to the reduced design domain. Over the 120 mm × 50 mm in-plane area, this corresponds to an equivalent areal heat input of approximately 8.33 kW/m$^2$. The prescribed heat rate represents the thermal loading assigned to the reduced-order model rather than the total losses of a complete electric machine. The same thermal and hydraulic boundary conditions are applied to all cases so that the resulting differences can be attributed primarily to topology evolution and the imposed regularization settings.

In addition to the thermal quantities, the hydraulic performance of each optimized topology is evaluated using the volumetric flow rate, hydraulic power, and hydraulic resistance. For the two-dimensional model, the volumetric flow rate is calculated by accounting for the prescribed out-of-plane thickness $L$,

$$Q_v = L \int u \cdot n \, d\Gamma, \tag{5}$$

where $\Gamma$ denotes the outlet boundary and $n$ is its outward unit normal vector. The hydraulic power associated with the imposed pressure difference is then defined as

$$P_{hyd} = \Delta p \cdot Q, \tag{6}$$

while the corresponding hydraulic resistance is evaluated as

$$R_h = \frac{\Delta P}{Q}. \tag{7}$$

Since the same pressure difference is prescribed for all optimization cases, the resulting volumetric flow rate and hydraulic resistance provide direct measures of the topology-dependent hydraulic conductance.

### 2.3. Topology optimization formulation

The optimization objective is to minimize the average temperature within the design domain:

$$minJ = T_{avg}, \tag{8}$$

where

$$T_{avg} = \frac{1}{A}\int T \, dA \tag{9}$$

and $A$ denotes the design-domain area.

The design variable $\rho \in \lfloor 0,1 \rfloor$ represents the local material state. Values close to zero correspond to fluid regions, while values approaching unity represent solid regions. A density-based interpolation scheme is employed to couple material distribution with fluid flow and heat transfer. The optimization process is performed under steady-state conditions, and no explicit volume fraction constraint is imposed.

### 2.4. AM-oriented regularization strategy

To improve manufacturability, three regularization mechanisms are employed.

First, a Helmholtz filter is introduced to enforce a minimum feature size and suppress mesh-dependent structures. The filter radius controls the characteristic length scale of the design field and suppresses features below a prescribed spatial scale. It therefore serves as a surrogate length-scale constraint for manufacturability, although it should not be interpreted as a direct specification of the minimum printable channel width.

Second, a Heaviside projection is applied to promote a near-binary material distribution. Increasing the projection parameter $\beta$ reduces intermediate-density regions and improves the physical interpretability of the optimized design [4].

**Table 1.** Parameters of the fluid and solid used in the simulation

| Parameter | Symbol | Value | Unit |
|---|---|---|---|
| Fluid density | $\rho_f$ | 1000 | kg/m$^3$ |
| Dynamic viscosity | $\mu_f$ | 0.001 | Pa · s |
| Thermal conductivity | $k_f$ | 0.6 | W/(m · K) |
| Specific heat capacity | $C_{p,f}$ | 4182 | J/(kg · K) |
| Solid density | $\rho_s$ | 7850 | kg/m$^3$ |
| Solid thermal conductivity | $k_s$ | 44.5 | W/(m · K) |
| Solid specific heat capacity | $C_{p,s}$ | 475 | J/(kg · K) |
| Maximum Brinkman coefficient | $\alpha_{max}$ | $4 \times 10^6$ | Pa · s/m$^2$ |

Third, a perimeter regularization term is incorporated into the objective function:

$$J = T_{avg} + \gamma \int |\nabla\theta|^2 \, d\Omega, \tag{10}$$

where $\theta$ denotes the filtered design field and is the perimeter penalty coefficient.

This term penalizes excessive interface length and discourages highly fragmented channel boundaries. Consequently, smoother and more continuous cooling channels are obtained, which are generally more compatible with AM processes.

### 2.5. Numerical setup and case definition

Five optimization cases (Cases A–E) are defined in Table 2. The corresponding optimized channel topologies and thermal fields are shown in Fig. 3 (Cases A–E).

The parameter sets listed in Table 2 were selected to provide progressively increasing levels of geometric regularization rather than to reproduce the manufacturing limits of a specific AM process. The filter radii of 0.3, 0.5, and 1.0 mm represent weak, moderate, and strong length-scale control within the present design domain. Increasing the filter radius progressively suppresses fine-scale branches and mesh-sensitive features. The projection parameter $\beta$ is increased from 1 to 3 together with the filtering strength to promote a sharper transition between the fluid and solid phases and to reduce intermediate-density regions.

The perimeter penalty coefficient $\gamma$ was selected from preliminary optimization tests to introduce a clear but non-dominant influence on interface complexity. A moderate value of $4 \times 10^{-7}$ is used in Case C to examine the effect of perimeter control under the intermediate filtering setting, whereas a 10-times larger value of $4 \times 10^{-6}$ is used in Case E to investigate the effect of stronger perimeter regularization under the strictest length-scale and projection settings. The selected cases therefore form a comparative regularization study rather than a calibration to a specific AM process. Case A serves as the weakly regularized reference, Case B introduces stronger length-scale and projection control, Case C additionally activates moderate perimeter regularization, and Cases D and E repeat this comparison under stronger filtering, with Case E representing the highest perimeter penalty level.

To quantitatively evaluate the resulting geometric complexity, a perimeter-based interface measure is calculated from the projected design field as

$$P = \int |\nabla\theta_p| d\Omega, \tag{11}$$

where $\theta_p$ denotes the projected material field. The relative perimeter $P/P_A$ is used to compare interface complexity among the optimized designs. In addition, the fluid area fraction is calculated. These quantities provide quantitative measures of geometric simplification and the change in available fluid area.

**Table 2.** Regularization parameters for the five optimization cases

| Case | Filter radius $R$ (mm) | Projection $\beta$ | Perimeter $\gamma$ |
|---|---|---|---|
| A | 0.3 | 1 | 0 |
| B | 0.5 | 2 | 0 |
| C | 0.5 | 2 | $4 \times 10^{-7}$ |
| D | 1.0 | 3 | – |
| E | 1.0 | 3 | $4 \times 10^{-6}$ |

### 2.6. Sharp-interface reanalysis

To assess the sensitivity of the optimized solution to the density-based Brinkman representation, Case B was reconstructed as a sharp fluid–solid geometry and reevaluated using conventional laminar flow and heat transfer physics without Brinkman penalization. The average temperature remained unchanged at 309 K, while the maximum temperature increased from 324 K to 335 K. The volumetric flow rate increased from 1.539 to 2.112 mL/s under the same 2 Pa pressure difference. These results indicate that the reduced-order TO model captures the global thermal response reasonably well, while local peak temperature and hydraulic conductance remain sensitive to the density-to-physics interpolation and interface reconstruction.

## 3. Results

### 3.1. Influence of feature size control

Cases A and B are first compared to investigate the influence of minimum feature size control on the optimized cooling channel topology.

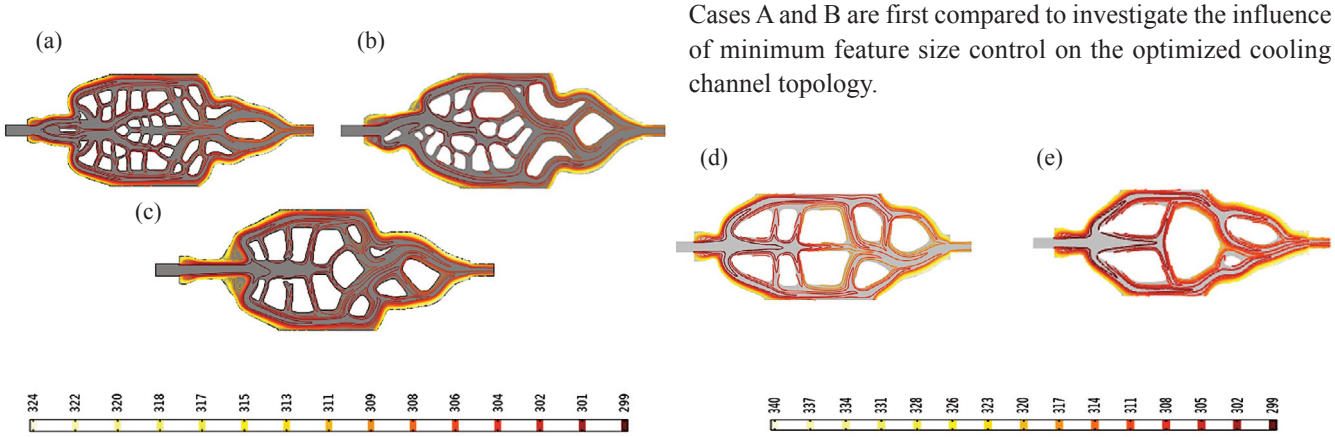



**Fig. 3.** Structural and thermal evolution of topology-optimized cooling channels under progressively strengthened manufacturability constraints. Representative isotherms are overlaid, temperature is in K. (a) Case A – weak constraint ($R$ = 0.3 mm, $\beta$ = 1), (b) Case B – feature size control ($R$ = 0.5 mm, $\beta$ = 2), (c) Case C – feature size + perimeter control ($R$ = 0.5 mm, $\beta$ = 2, $\gamma = 4 \times 10^{-7}$), (d) Case D – strong constraint ($R$ = 1 mm, $\beta$ = 3), (e) Case E – feature size + strong perimeter control ($R$ = 1 mm, $\beta$ = 3, $\gamma = 4 \times 10^{-6}$).

**Table 3.** Thermal and hydraulic performance of the optimized designs

| Case | $T_{avg}$ (K) | $T_{max}$ (K) | $Q$ (mL/s) | $P_{hyd}$ (μW) | $R_h$ ($10^6$) Pa · s/m$^3$) |
|---|---|---|---|---|---|
| A | 303 | 317 | 1.764 | 3.528 | 1.134 |
| B | 309 | 324 | 1.539 | 3.077 | 1.300 |
| C | 306 | 321 | 1.214 | 2.428 | 1.648 |
| D | 312 | 330 | 1.030 | 2.059 | 1.942 |
| E | 316 | 339 | 1.014 | 2.029 | 1.972 |

Under weak regularization (Case A), the optimizer is allowed to exploit a large geometric design space. As shown in Fig. 3a, the resulting topology consists of a highly branched porous network containing numerous small-scale channels and local flow paths. Such structures significantly increase the fluid–solid interface area and promote distributed convective heat transfer throughout the domain.

When the filter radius is increased from 0.3 mm to 0.5 mm, and the projection parameter is increased from 1 to 2 (Case B), many of these fine structures are suppressed. The topology evolves toward a smaller number of dominant flow channels with improved geometric clarity. However, this simplification reduces the available heat transfer area and limits local flow redistribution.

The thermal degradation is accompanied by a clear change in hydraulic behavior. As the filter radius and projection strength are increased from Case A to Case B, the volumetric flow rate decreases from 1.764 to 1.539 mL/s under the same imposed pressure difference of 2 Pa. Accordingly, the hydraulic resistance increases from $1.134 \times 10^6$ to $1.300 \times 10^6$ Pa · s/m$^3$. At the same time, the average temperature increases from 303 K to 309 K, and the maximum temperature rises from 317 K to 324 K, as summarized in Table 3. These results indicate that stronger feature size control suppresses small-scale parallel flow paths, thereby reducing both the hydraulic conductance and the geometric freedom available for thermal optimization.

### 3.2. Effect of perimeter regularization

To further improve manufacturability, a perimeter regularization term is introduced in Cases C and E.

For the moderate filtering setting (Cases B and C), the perimeter penalty promotes the formation of smoother and more continuous channel boundaries. Compared with Case B, the optimized topology in Case C exhibits fewer fragmented structures and a more organized channel network. Interestingly, despite the additional geometric restriction, the average temperature decreases from 309 K to 306 K, and the maximum temperature decreases from 324 K to 321 K. This thermal improvement does not result from an increased coolant flow rate. On the contrary, the volumetric flow rate decreases from 1.539 mL/s in Case B to 1.214 mL/s in Case C, corresponding to an increase in hydraulic resistance from $1.300 \times 10^6$ to $1.648 \times 10^6$ Pa · s/m$^3$. The result therefore suggests that moderate perimeter regularization can improve the spatial organization of the cooling paths even when the overall hydraulic conductance is reduced. In particular, the suppression of thermally inefficient local branches may redistribute the available coolant toward more effective heat transfer regions. One isolated branch remains in Case C, where a secondary low-density region is disconnected from the primary flow network. This feature may result from the competition between thermal optimization and perimeter minimization. Establishing an additional connection would increase the fluid–solid interface length and hence the perimeter penalty, while providing only a limited thermal benefit. The optimizer may therefore retain the local feature without forming a complete hydraulic connection.

### 3.3. Behavior under stronger regularization

To examine whether the observed influence of perimeter regularization remains valid under stricter manufacturability constraints, two additional cases are considered using a larger filter radius of 1 mm and a projection parameter of 3.

Without perimeter regularization, Case D yields an average temperature of 312 K and a maximum temperature of 330 K. Introducing the stronger perimeter penalty in Case E further simplifies the channel geometry and suppresses secondary branches. However, the average temperature increases to 316 K, and the maximum temperature rises to 339 K. In contrast to the pronounced thermal deterioration, the volumetric flow rate changes only slightly, from 1.030 mL/s in Case D to 1.014 mL/s in Case E, while the hydraulic resistance increases from $1.942 \times 10^6$ to $1.972 \times 10^6$ Pa · s/m$^3$. The comparatively small hydraulic change indicates that the thermal degradation cannot be attributed primarily to a reduction in the total coolant flow rate. Instead, the stronger perimeter penalty appears to eliminate secondary heat transfer pathways and reduce the effective fluid–solid interfacial area. This result further indicates that excessive geometric regularization can compromise thermal performance even when the overall hydraulic resistance changes only marginally.

### 3.4. Thermal–hydraulic–manufacturability trade-off

The combined results reveal that manufacturability-oriented regularization affects not only the thermal behavior but also the hydraulic characteristics of the optimized cooling channels. As the geometric constraints are progressively strengthened from Case A to Case E, the volumetric flow rate decreases from 1.764 to 1.014 mL/s under the same prescribed pressure difference, while the hydraulic resistance increases from $1.134 \times 10^6$ to $1.972 \times 10^6$ Pa · s/m$^3$. Thus, the progressive simplification of the topology does not imply a reduction in flow resistance; instead, suppressing fine-scale and parallel flow paths can reduce the overall hydraulic conductance of the channel network.

The corresponding hydraulic power decreases from 3.528 to 2.029 μW because the pressure difference is fixed in all

**Table 4.** Quantitative geometric characteristics of the optimized designs

| Case | $P$ (m) | $P/PA$ | Fluid fraction |
|---|---|---|---|
| A | 0.75378 | 1 | 0.415 |
| B | 0.59941 | 0.795 | 0.367 |
| C | 0.51426 | 0.682 | 0.346 |
| D | 0.47877 | 0.635 | 0.336 |
| E | 0.13969 | 0.185 | 0.159 |

cases, and $P_{hyd} = \Delta pQ$. This reduction should therefore not be interpreted as improved hydraulic performance. Under the present pressure-driven boundary condition, a lower hydraulic power primarily reflects the lower volumetric flow rate resulting from the increased hydraulic resistance.

The thermal response is not governed by flow rate alone. The comparison between Cases B and C shows that moderate perimeter regularization can reduce both the average and maximum temperatures despite a lower total flow rate, indicating that improved spatial organization of the coolant pathways may partially compensate for the loss of hydraulic conductance. In contrast, the comparison between Cases D and E shows substantial thermal degradation despite only a minor change in flow rate, suggesting that excessive regularization removes heat transfer pathways that remain thermally beneficial.

The quantitative geometric measures in Table 4 confirm the visual simplification of the optimized layouts. The perimeter measure decreases progressively from 0.754 m in Case A to 0.140 m in Case E, corresponding to an 81.5% reduction in interface complexity relative to the weakly regularized reference. The fluid area fraction simultaneously decreases from 0.415 to 0.159. Therefore, stronger regularization not only suppresses fragmented interfaces but also reduces the available fluid region. This combined change helps explain the increase in hydraulic resistance and the thermal degradation observed under the strongest regularization settings.

These observations demonstrate that the AM-oriented design problem involves a coupled trade-off among geometric simplicity, hydraulic conductance, and thermal performance. Manufacturability constraints should therefore be selected to control geometric complexity without unnecessarily suppressing thermally effective flow structures.

## 4. Discussion and conclusion

The results demonstrate that AM-oriented regularization affects the optimized cooling channels through a coupled trade-off among geometric complexity, thermal performance, and hydraulic behavior. Increasing the filter radius, projection strength, and perimeter penalty progressively suppresses fine-scale branches and fragmented boundaries, producing smoother and more manufacturable channel layouts. However, geometric simplification does not necessarily improve thermo-fluid performance.

A sharp-interface reanalysis of Case B was additionally performed to assess the sensitivity of the optimized solution to the density-based Brinkman representation. The reconstructed geometry reproduced the average temperature of the TO model, while the maximum temperature increased from 324 K to 335 K, and the volumetric flow rate increased from 1.539 to 2.112 mL/s. The agreement in the average temperature indicates that the reduced-order model captures the global thermal response reasonably well. However, the differences in the peak temperature and hydraulic conductance show that local thermo-fluid behavior remains sensitive to the density-to-physics interpolation and the reconstruction of the fluid–solid interface.

An important observation is that geometric simplicity and hydraulic efficiency are not equivalent. The weakly regularized designs contain multiple interconnected and approximately parallel flow paths, which can provide relatively high hydraulic conductance despite their greater geometric complexity. As regularization is strengthened, the reduction in available parallel flow paths leads to a progressive decrease in flow rate and a corresponding increase in hydraulic resistance. The corresponding decrease in hydraulic power therefore results from the lower flow rate under the constant-pressure boundary condition and should not be interpreted as improved hydraulic performance.

The thermal response is also not governed by total flow rate alone. From Case B to Case C, the flow rate decreases while both the average and maximum temperatures are reduced, suggesting that moderate perimeter regularization may improve the spatial organization of the cooling paths and suppress thermally inefficient local branches. In contrast, the flow rate changes only slightly from Case D to Case E, whereas the thermal performance deteriorates markedly. This indicates that excessive regularization can remove secondary heat transfer pathways and reduce the effective fluid–solid interfacial area even when the overall hydraulic resistance changes only marginally.

The present AM-related constraints should be interpreted as geometric regularization mechanisms rather than a complete representation of a specific AM process. The model does not explicitly include build orientation, overhang limits, support requirements, powder removal, residual stress, thermal distortion, or material anisotropy. In addition, the two-dimensional cold plate model is intended as a reduced-order topology development platform and does not reproduce through-thickness flow redistribution or three-dimensional manifold effects in a practical motor water jacket.

Finally, hydraulic performance is currently evaluated only as a post-optimization quantity, while the objective function minimizes the average temperature without an explicit pressure drop or pumping power constraint. Future work will therefore extend the framework to three-dimensional water jacket geometries and multi-objective formulations that simultaneously consider thermal performance, hydraulic losses, and process-specific AM constraints.

### Data availability statement

The datasets used and/or analyzed during the current study are available from the corresponding author at reasonable request.

**Acknowledgment**

The publication costs of this article were covered by the Estonian Academy of Sciences.

## References

1. Zhang, B., Qu, R., Fan, X. and Wang, J. Thermal and mechanical optimization of water jacket of permanent magnet synchronous machines for EV application. In *Proceedings of the 2015 IEEE International Electric Machines & Drives Conference* (*IEMDC*), *Coeur d'Alene, ID, USA, 10–13 May 2015*. IEEE, 2015, 1329–1335. https://doi.org/10.1109/IEMDC.2015.7409234
2. Ye, Z.-N., Luo, W.-D., Zhang, W.-M. and Feng, Z.-X. Simulative analysis of traction motor cooling system based on CFD. In *Proceedings of the 2011 International Conference on Electric Information and Control Engineering, Wuhan, China, 15–17 April 2011*. IEEE, 2011, 746–749. https://doi.org/10.1109/ICEICE.2011.5777373
3. Liu, Z., Zhao, H., Qiu, Y., Zeng, H. and Dong, X. Numerical analysis of topology-optimized cold plates for thermal management of battery packs. *Applied Thermal Engineering*, 2024, **238**, 121983. https://doi.org/10.1016/j.applthermaleng.2023.121983
4. Guest, J. K., Prévost, J. H. and Belytschko, T. Achieving minimum length scale in topology optimization using nodal design variables and projection functions. *International Journal for Numerical Methods in Engineering*, 2004, **61**(2), 238–254. https://doi.org/10.1002/nme.1064

## Elektrimasinate vesijahutussärkide jahutuskanalite lisatootmist arvestav topoloogia optimeerimine vähendatud järgu külmplaadimudeli abil

**Yang Zhang, Martin Sarap, Toomas Vaimann ja Ants Kallaste**

Suure võimsustihedusega elektrimasinate soojusjuhtimisel kasutatakse laialdaselt vedelikjahutusega vesijahutussärke, kuid tavapärased jahutuskanalite lahendused põhinevad sageli ettemääratud geomeetrilistel konfiguratsioonidel. Lisatootmine võimaldab valmistada keerukamaid sisemisi jahutusstruktuure ja loob võimaluse kasutada topoloogia optimeerimist nende efektiivsemaks kujundamiseks. Käesolevas töös esitatakse lisatootmist arvestav jahutuskanalite topoloogia optimeerimise meetod, mis põhineb elektrimasina vesijahutussärgi vähendatud järgu kahemõõtmelisel külmplaadimudelil. Meetodis kasutatakse tiheduspõhist topoloogia optimeerimist koos Helmholtzi filtreerimise, Heaviside'i projektsiooni ja perimeetri regulaarimisega. Viie optimeerimisjuhu abil uuritakse regulaarimise mõju jahutuskanalite geomeetriale, termilisele jõudlusele ja hüdraulilisele käitumisele. Tulemused näitavad, et regulaarimise tugevdamine vähendab oluliselt geomeetrilist keerukust ja vedelikuosa, kuid suurendab üldjuhul hüdraulilist takistust ja halvendab termilist jõudlust. Samal ajal võib mõõdukas perimeetri regulaarimine parandada jahutuskanalite ruumilist paiknemist ja vähendada keskmist temperatuuri. Lisaks viidi läbi ühe optimeeritud lahenduse terava liidesega kordusarvutus, mis näitas head kooskõla globaalse termilise vastuse osas, kuid tõi esile lokaalse tipptemperatuuri ja hüdraulilise juhtivuse tundlikkuse tiheduspõhise mudeli suhtes. Tulemused näitavad, et lisatootmist arvestav topoloogia optimeerimine võimaldab süstemaatiliselt uurida kompromissi termilise jõudluse, hüdraulilise käitumise ja valmistatavuse vahel.